Carpathian Journal of Earth and Environmental Sciences, August 2026, Vol. 21, No. 2, p. 381 – 394; DOI:10.26471/cjees/2026/021/376

PETRO-MINERALOGICAL AND GEOCHEMICAL ANALYSIS OF THE IRON MINERALISATION AT KEF BOULEHMAME, JIJEL, NE-ALGERIA. CONTRIBUTION OF STABLE CARBON AND OXYGEN ISOTOPES

Azzouz BENLAMARI[1,2], Rabah ZEDAM[1,3*], Abdelmalek LEKOUI[2,4], Toufik BATOUCHE[5] & Safia SAOULI[6]

[1] Department of Geology, Faculty of Earth Sciences and Architecture, Larbi Ben M'hidi University, Oum El Bouaghi, Algeria. E-mails: (A.B) benlamari.azzouz@univ-oeb.dz; (R.Z) zedam.rabah@univ-oeb.dz

[2] Department of Earth and Universe Sciences, Faculty of Natural and Life Sciences, Mohammed Seddik Ben Yahya University, Jijel, Algeria. E-mails: (A.B) azzouz.benlamari@univ-jijel.dz ; (A.L) lekouim121@gmail.com

[3] Water Resources Mobilization and Management Laboratory, Batna 2 University.

[4] Laboratory of Geological Engineering (LGG), Faculty of Natural and Life Sciences, University of Jijel, 18000, Jijel, Algeria. E-mail: lekouim121@gmail.com

[5] Department of Mining Engineering, Laboratory of Mines, Metallurgy and Materials L3M, National Higher School of Technology and Engineering, 23005 Annaba, Algeria. E-mail: t.batouche@ensti-annaba.dz

[6] Underground Reservoir Laboratory: Oil, Gas and Aquifers. Kasdi Merbah University-Ouargla, 30000, Algeria. E-mail: saoulisafia@univ-ouargla.dz

**Corresponding author: zedam_rabah@yahoo.fr*

Abstract: Kef Boulehmame is a carbonate massif belonging to the Tellian zone of the Alpine orogeny in northeastern Algeria. Covering approximately 10 km², it is bordered to the north and northeast by the Paleozoic metamorphic basement and forms an elongated dome extending in a NNW–SSE direction. This Jurassic-age massif is characterized by a thick limestone sequence (800 m), with rare dolomitic interbeds, exhibiting a dome-like structure traversed by two main fault systems-oriented NW–SE and NNE–SSW. The iron-bearing mineralization hosted within these microcrystalline limestones of the lower Lias occurs as clusters and veins ranging in size from tens of centimeters to meters, with a surface extent of several meters. Our study aimed to characterize this mineralization from petro-mineralogical and geochemical perspectives using a multidisciplinary approach: microscopic analysis, X-ray diffraction, X-ray fluorescence, and the analysis of stable isotopes (C, O) to identify the mineralization and origin of the mineralizing fluid. The petro-mineralogical study revealed various iron oxides and hydroxides (hematite, goethite, and limonite) associated with gangue minerals (calcite, quartz, and barite) in the presence of metallic mineralization (bornite and tennantite/tetrahedrite), as well as a supergene alteration phase (malachite/azurite). Geochemical analyses revealed a high Fe_2O_3 content (84.73%), with significant proportions of CaO (10.75%) and SiO_2 (10.52%), as well as notable enrichment in metallic trace elements (Cu, Zn, Pb, and As) and non-metallic elements (Ba and S), probably reflecting late-stage hydrothermal circulation responsible for the baryte–sulphide–sulfosalt association. The analysis of stable isotopes of carbon and oxygen (C and O), conducted on calcite–ankerite gangue minerals, showed $\delta^{13}C$ PDB values ranging from −2.01 ‰ to +3.537 ‰, suggesting an inorganic origin for the carbon, probably derived from the thermal decarbonation of the surrounding limestone rocks. Simultaneously, the $\delta^{18}O$ SMOW values obtained ranged from +18.21 ‰ to +28.65 ‰, indicating the effect of high temperatures, probably caused by the circulation of deep hydrothermal fluids. Overall, the results supported the hypothesis that hydrothermal remobilization is responsible for this iron-bearing mineralization.

Keywords: Kef Boulehmame, Lias limestone, iron mineralisation, goethite, hydrothermal fluids, stable isotopes (C-O).

1. INTRODUCTION

Multiple geological processes spanning the Archean to the Cenozoic eon govern the formation of iron ore deposits. From an economic viewpoint, the most significant iron deposits include banded iron formations

(BIF), magmatic and hydrothermal iron deposits, and lateritic and sedimentary iron accumulations (Zhao et al., 2014; Cooper et al., 2018; Mallinger and Mergili, 2020; Idoine et al., 2022). Banded iron formations (BIF) are of particular interest due to their large size; they are predominantly associated with Precambrian shields in several countries, including Australia, Brazil, Russia, and South Africa. Conversely, hydrothermal iron deposits, commonly associated with magmatism and well-developed in China, Chile, and Iran, are typically confined to orogenic belts (Bekker et al., 2010; Zhao et al., 2021). From an academic perspective, it is necessary to identify the geological and petrogeochemical characteristics of this natural resource. Hence, the application of stable isotope analyses of iron, carbon, and oxygen is crucial for characterizing the mineralizing fluids of this type of deposit and for providing key insights into the thermodynamic conditions of their formation and chemistry (Wang et al., 2019; Heimann et al., 2020).

Globally, iron ore consumption is rapidly increasing, which has further stimulated exploration efforts and the re-evaluation of reserves in known deposits through the application of modern analytical techniques (Chaib et al., 2024; Liu & Lin, 2024). Algeria possesses significant iron ore reserves, the mining of which dates back to the colonial era. This mining is a cornerstone of the national extractive economy and represents a major geostrategic asset. However, many prospects and deposits are currently inactive, pending further technical and economic reassessment (Mowafa, 2014, 2018; Bouchair et al., 2021). The iron ore deposits of northeastern Algeria have formed within various structural and lithological settings, ranging from peridiapiric mineralization in the Mellegue mountains (Boukhadra, Ouenza, and Djebel Had) to skarn systems in northern Constantine (Edough and Aïn Sedma). The work conducted on these mineral deposits has helped refine the understanding of the processes involved in their formation and development (Bouzenoune & Lécolle, 1997; Aïssa et al., 1998; Bouftouha, 2000; Aït Abdelouahab et al., 2011; Bouhlel et al., 2016; Diab et al., 2020). Conversely, the deposits in the Tellian mountain range, particularly those at Sidi Marouf and Kef Boulehmame, are inadequately documented in the scientific literature, despite their unique tectonic location and economic potential. The recently established steelworks (Algerian Qatari Steel, AQS), located near the two aforementioned deposits, could make the region a new hub for iron ore production.

This study aimed to contribute to the petrogeochemical investigation of the iron-bearing mineralization at Kef Boulehmame, using a multidisciplinary approach combining several analytical methods: X-ray diffraction (XRD), X-ray fluorescence (XRF), inductively coupled plasma optical emission spectrometry (ICP-OES), and the analysis of stable C and O isotopes in gangue carbonates. It focused on identifying the mineral assemblages present, geochemically characterizing the ore and its gangue, and determining the origin of the mineralizing fluids.

2. GEOLOGICAL SETTING

The Kef Boulehmame iron deposit forms part of the large Moul Ed Demamène massif, located 8 km south of El-Milia. Discovered in 1921 along a major fault placing Middle Lias limestones in contact with lower Cretaceous marls, the deposit contains estimated reserves of 650,000 tons, with an iron content of 53% (Sonarem, 1974). The iron mineralization occurs as metric-scale hematite veinlet networks, generally striking NNE–SSW and hosted within the limestone host rock.

It occasionally appears as spheroidal masses of iron oxides and hydroxides, hosted (embedded) in dark limestones containing chert (flint) nodules. These structures suggest the probable existence of residual iron-rich pockets, which could represent significant potential for future exploration. The Moul Ed Demamène massif forms a tectonic half-window, revealing a stack of ancient structural units deposited prior to the upper Oligocene (Durand-Delga 1955, Durand-Delga et al., 2000). From top to bottom, the stratigraphic sequence reveals the following succession (Figure 1-a): Border Nappe (Paleozoic metamorphic basement), Upper dolomitic slice (Malm) of Draa El Kasba, Middle Jurassic slice of Kef Boulehmame, Lower slice of the "Kefs" with folded structures, Supernumerary slice of El Akbia (upper Cretaceous), and Autochthonous unit featuring overturned flyschs overlying Senonian marls. The massif in question exhibits a two-tiered dome-like structure (Bouillin, 1977; Vila, 1980):

- An upper, epimetamorphic tier comprising the Sidi Ahmed, Sidi Rhiat, and Achaiches units.
- A lower tier comprising the Kef Boulehmame and Draa El Kasba slices (Figure 1-b).

From a lithostratigraphic perspective, the massif exhibits a wide variety of facies. The Paleozoic metamorphic basement comprises augen gneiss, which is occasionally granulitic, as well as schists and crystalline limestones with intercalations of quartz-rich mica schists. This basement is clearly cross-cut by an intrusive complex comprising gabbros, dolerites, and altered basalts.

The Triassic strata comprise a broad diapiric body trending NW–SE, comprising variegated marls interbedded with detrital layers, featuring yellowish clay and compact gypsum masses. The Jurassic constitutes the majority of the Kef Boulehmame, characterized by carbonate series forming a dome-like segment globally

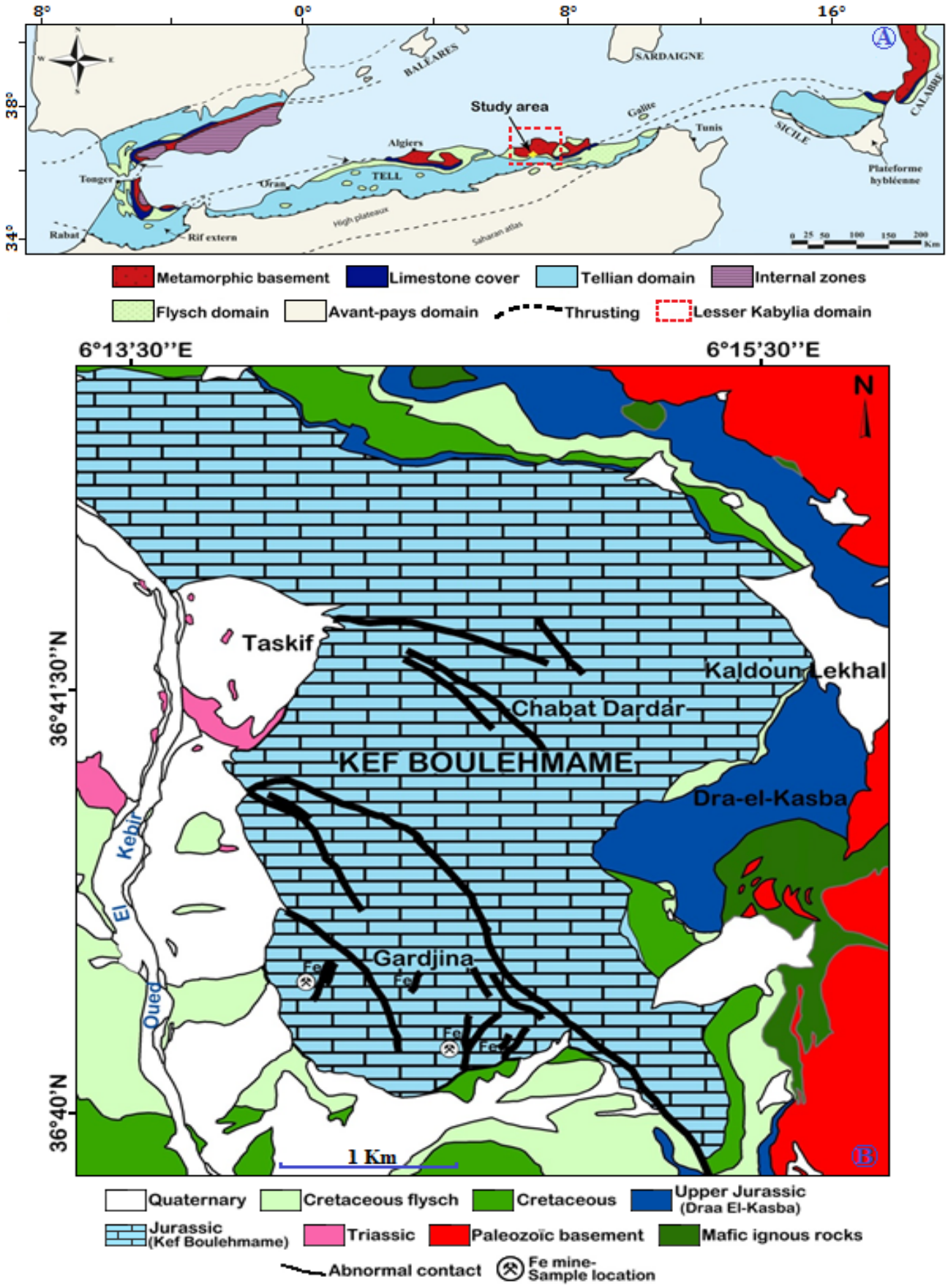

Figure 1. (a) Simplified structural map of the Alpine orogen showing the location of the study area (Durand-Delga et al., 2000, modified); (b) Schematic geological map of Kef Boulehmame and its immediate surroundings (Durand-Delga, 1969, modified).

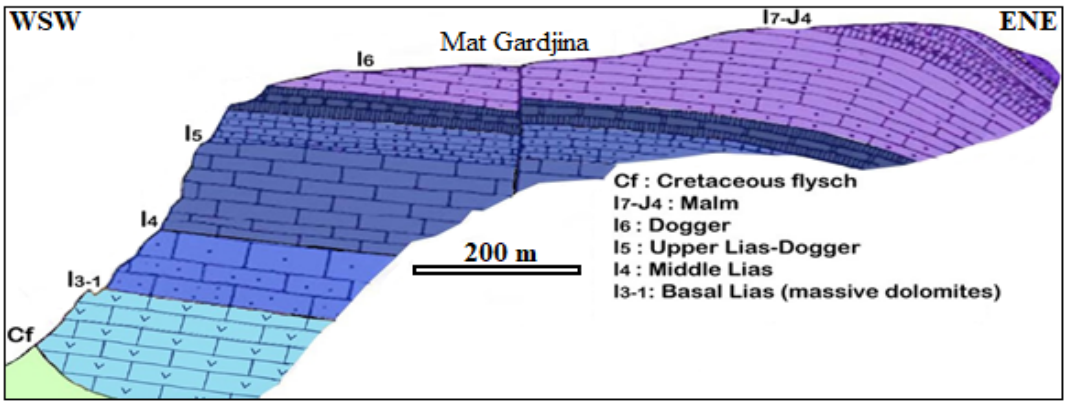

Figure 2. Synthetic section of the Jurassic carbonate series at Kef Boulehmame (Durand-Delga, 1955; Bouillin, 1977; modified).

oriented NNW–SSE, reaching a height of 860 m. At its base are massive Liassic dolomites (100 m thick), which are well developed in the northern part (Figure 2). They are overlain by microcrystalline bluish limestones of the Middle Lias (250 to 300 m), containing iron mineralization. At the top, these limestones are replaced by siliceous facies, overlain by spathic limestones with interbeds of marl containing detrital debris.

The Lias–Dogger transition is represented by a 60-meter-thick sequence of bluish marls, arranged in centimeter thick layers. The Malm consists of light-colored siliceous limestones, more compact at the top. The Cretaceous formations are discordant and divided into two distinct facies: (a) the more prevalent Tellian type, comprising detrital limestones, marls, and pebble conglomerates (Durand-Delga, 1955, 1969), and (b) the less prevalent Massylian flysch type, comprising schists, sandy flysch, and quartzites, reflecting an environment linked to the Alpine orogeny (Bouillin, 1977).

Finally, the most recent formations, such as Quaternary alluvium and scree (talus), are primarily developed along the Oued El-Kébir. From a tectonic perspective, the Kef Boulehmame locality is characterized by a complex network of multidirectional faults, which probably facilitated the circulation of hydrothermal fluids during a succession of several tectonic phases. The NW–SE (Chaabet Dardar) and N–S (western massif) faults are pre-Oligocene and exhibit Triassic gypsiferous injections. Conversely, the post-Oligocene tectonic phase resulted in the development of brittle structures (the Gardjina fault), oriented NW–SE and characterized by variable and limited displacements. To the south of the massif, the NNE–SSW faults follow the same direction as the iron-mineralized veins.

3. MATERIALS AND METHODS

A representative systematic sampling was meticulously conducted, targeting the various ore bodies of the iron deposit (veins, pockets, and old adits) as well as the limestone host rock in the immediate vicinity of the mineralization. After sorting, cleaning, and washing in the laboratory, the selected samples were initially examined under a binocular microscope to establish the final analytical procedure.

An initial set of samples was selected for the preparation of thin sections and polished sections, which were examined under transmitted light microscope and reflected light microscope (Zeiss Axiolab Double Light), respectively as part of the petro-mineralogical and metallographic analysis. This study enabled the determination of the deposit's petrographic and mineralogical inventory, as well as all its mineral associations, allowing the establishment of a paragenetic sequence.

A second set of samples was sent for X-ray diffraction (XRD) analysis at the Center for Scientific and Technical Research in Physico-Chemical Analysis (CRAPC) in Biskra, Algeria. The powders obtained using a Humboldt Wedag roller mill were analyzed using a Bruker D8 X-ray diffractometer with Cu Kα radiation ($\lambda = 1.5406$ Å) and an angular sweep from 5° to 90° (2θ). The diffractograms obtained are analyzed using X'Pert HighScore Plus software. This semi-quantitative analysis is used as a complement to microscopic observation, to identify the main mineral phases.

The third batch of samples was reserved for X-ray fluorescence (XRF) analysis, using a Panalytical Zetium XRF analyzer, as well as inductively coupled plasma optical emission spectrometry (ICP-OES). This series of analyses aimed to quantify the composition of metallic and non-metallic elements at varying concentrations, ranging from major to trace elements. It was conducted simultaneously at the CRAPC in Biskra and at the geology and geochemistry laboratory at the ORGM (Office de Recherche Géologique et Minière) in Boumerdes, Algeria.

Finally, a set of eight samples comprising gangue carbonates (calcite and ankerite) and intact Jurassic-age host limestones was subjected to stable isotope analysis of carbon ($\delta^{13}C$) and oxygen ($\delta^{18}O$). This analysis aimed to determine the origin and chemistry of the

mineralizing fluid responsible for the formation of this iron-bearing mineralization at Kef Boulehmame. These analyses were conducted at the isotopic geochemistry laboratory of the Institute of Geology and Mineralogy at the University of Cologne (Germany), using a Thermo Finnigan MAT 252 mass spectrometer coupled with an equilibration bench.

4. RESULTS

4.1. Host Rock Petrography

The petro-mineralogical study of the Lias limestone host showed that it comprised very hard, gray-blue, finely crystalline micrites, with conchoidal fractures, arranged in decimeter- to meter-thick beds, indicating a platform depositional environment (Folk, 1959; Dunham, 1962).

These micrites are crisscrossed by a dense network of fractures filled with late-stage palissadic calcite, associated with iron oxides, black flint nodules, and rare idiomorphic pyrite grains (Figure 3-a, Figure 3-b). Microscopic examination of the micritic matrix reveals the presence of two distinct microfacies: one is a mudstone with few fossils, and the other is a wackestone rich in bioclastic fragments (ostracods, gastropods, and foraminifera), (Figure 3-c, Figure 3-d).

4.2. Mineralization

Macroscopic and microscopic observations revealed that the Kef Boulehmame iron deposit exhibited a rich and diverse mineralogical cortex associated with the iron ore and its host rocks. In order of predominance, the deposit showed a mineral assemblage comprising the ferriferous mineralization zone, sulfides and sulfosalts, gangue minerals, and supergene alteration minerals.

4.2.1. Ferriferous Mineralization

Hematite. Main mineral, with a massive appearance, occurring in large irregular centimeter to decimeter-sized patches or in box-work, most often filling fractures and voids in the host rocks, probably indicating an initial mineralization phase established under high-temperature conditions (Figure 4-b, Figure 4-e).

Goethite. Often associated with hematite, occurring in botryoidal form or as colloform hematite-goethite banding. It may result from secondary low-temperature enrichment under more oxidizing conditions or represent the alteration of earlier phases (Figure. 4-d).

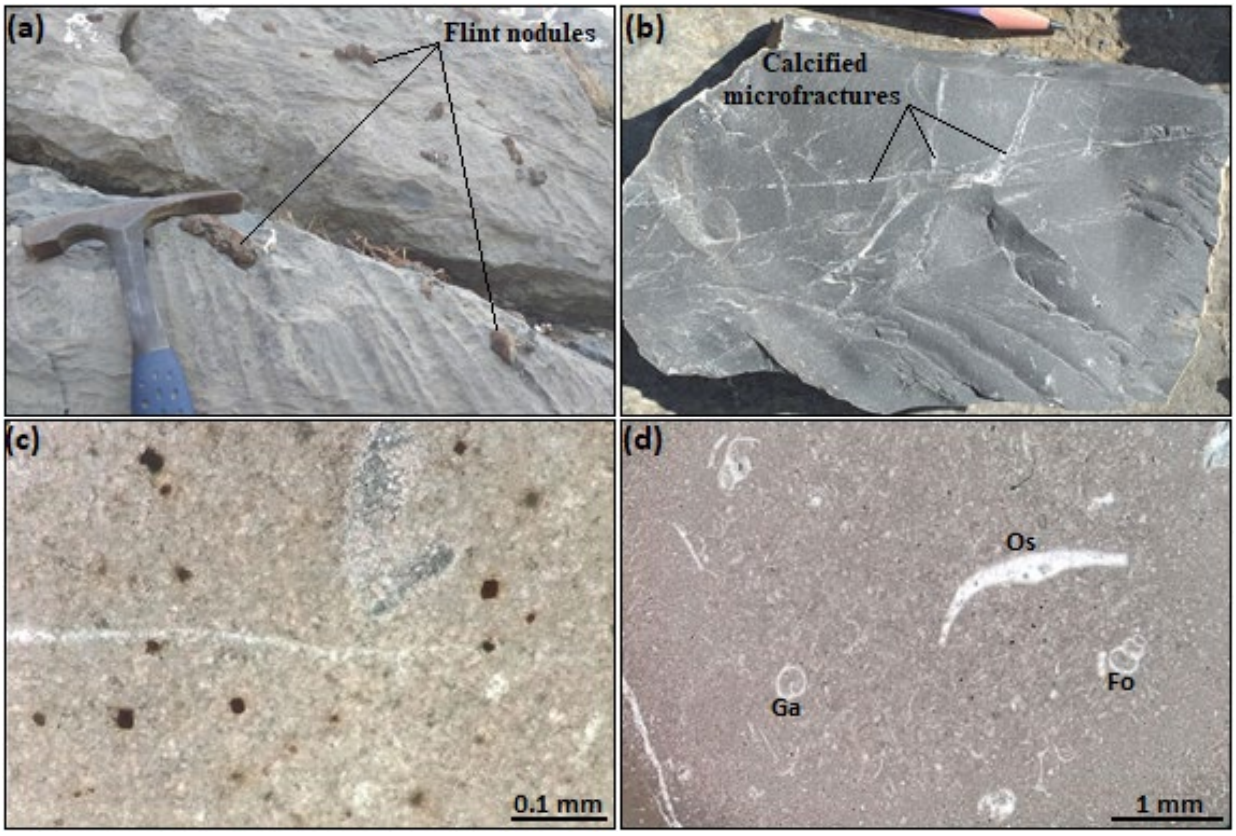

Figure 3. Macroscopic and microscopic features of the Lias limestone host rock of the Kef Boulehmame iron mineralization: (a) Limestone with black flint nodules; (b) Highly fractured micritic limestone with calcitic filling (calcified microfractures); (c) Mudstone with idiomorphic crystals of pyrite and iron oxides (black grains); (d) Wackestone containing ostracods (Os), foraminifera (Fo), and gastropods (Ga).

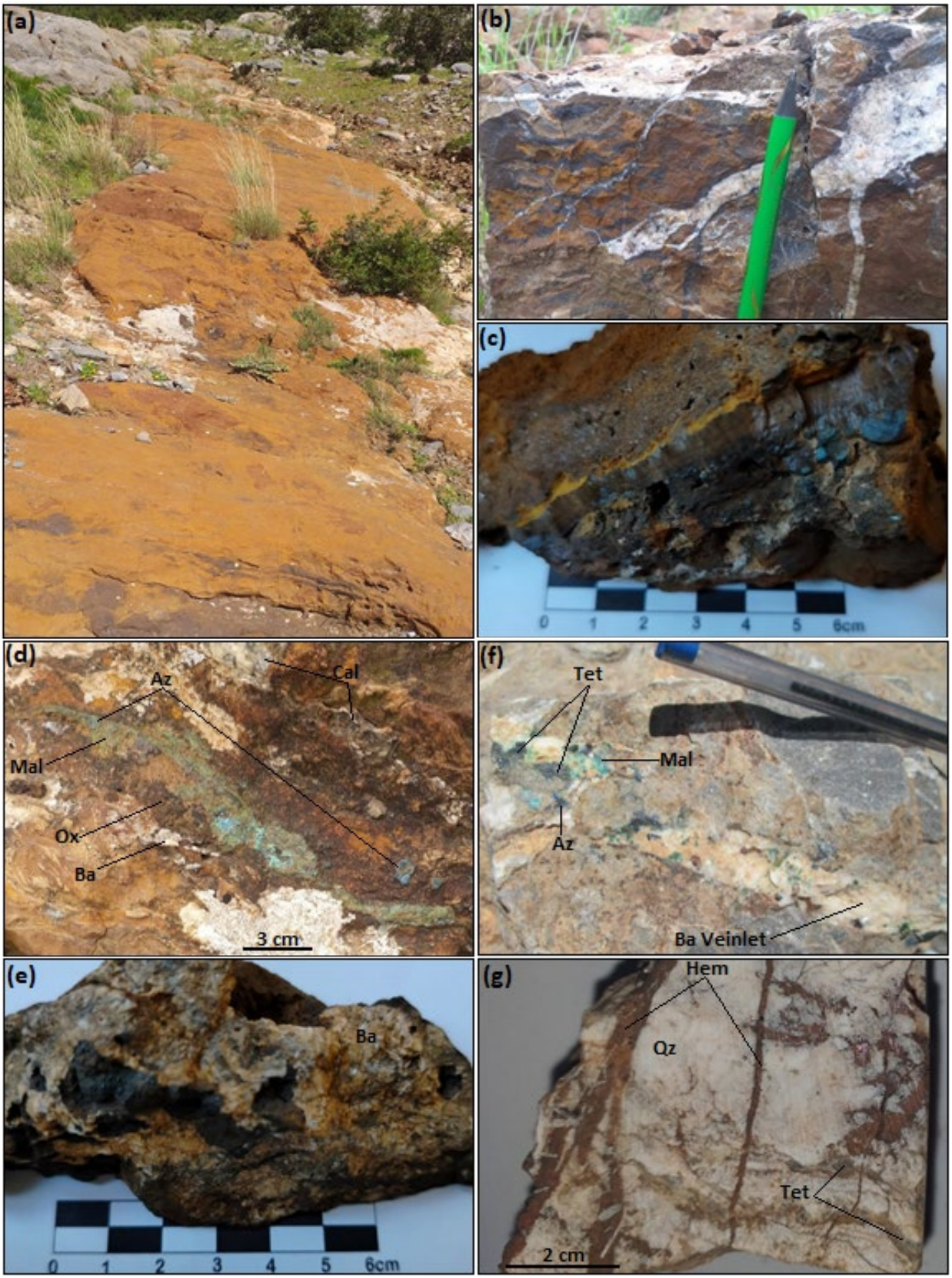

Figure 4. Morphology and textures of the iron-bearing mineralization at Kef Boulehmame: (a) Mineralized body in a sill-bedded formation ; (b) Stockwork veined iron mineralization ; (c) Collomorphic aspect of the hematite (Hem) – goethite (Goet) – ankerite (Ank) association; (d) Mineral association of iron oxides (Ox) – malachite (Mal) – azurite (Az) – calcite (Cal) – barite (Ba); (e) Fine sheaf-like crystals of barite (Ba) associated with iron oxides and hydroxides; (f) Tetrahedrite (Tet) – malachite (Mal) – azurite (Az) disseminated in a barite (Ba) veinlet; (g) Stockwork microfractures filled with hematite (Hem) and tetrahedrite (Tet).

4.2.2. Sulfides and Sulfosalts

Tetrahedrite. Occurred as rare, tiny millimeter-sized grains disseminated in barite, sometimes in veinlets associated with iron oxy-hydroxides in quartz patches. The mineral-exhibited centimeter-scale iridescence, altered to malachite and azurite. (Figure 4-f, Figure 4-g).

Pyrite. Found as rare framboidal or idiomorphic crystals, more or less oxidized, millimeter-sized, and scattered in the carbonate host around mineralized bodies. The scarcity of these primary sulfides is consistent with an oxidizing environment, probably related to near-surface conditions or circulation of oxidized fluids in a highly fractured context.

Bornite. Rarely observed macroscopically, it was detected by X-ray diffraction in three ferriferous ore samples. Its presence may indicate a minor early sulfide phase, largely reworked by supergene alteration.

4.2.3. Gangue Minerals

Calcite. The main gangue mineral, occurring as millimeter-sized saccharoidal crystals, often with a drusy texture. Calcite is associated with iron ore, filling fractures, cementing mineralized breccias, and forming banded structures within ore–calcite aggregates (Figure 4-d, Figure 5-b, Figure 5-f).

Quartz. Appeared sporadically as small centimeter-sized masses associated with fracture networks filled with iron oxy-hydroxides and tetrahedrite (Figure 5-d). Quartz was systematically detected by XRD.

Barite. Occurred in two generations: (a) first generation in tabular, palisade-structured crystals corroded by iron oxy-hydroxides, suggesting early or syngenetic emplacement; (b) second generation as small, radiating crystal bundles coating iron oxy-hydroxides, representing a late-stage emplacement (Figure 4-d, Figure 4-e, Figure 4-f, Figure 5-c).

4.2.4. Supergene Alteration Minerals

Limonite. Ubiquitous, with a clumpy or sometimes powdery appearance, masking other oxides. It represented a very late supergene alteration phase (Figure 4-d, Figure 4-e).

Malachite/azurite. Occurred either as alteration halos around centimeter-scale tetrahedrite grains or as tiny crystals disseminated within the hematitic mass (Figure 4-d, Figure 4-f, Figure 5-e).

4.3. XRD results

X-ray diffraction analysis showed the predominance of two main mineral phases, reflecting the iron-rich nature of the ore and the lithology of the host rock, which comprised hematite and calcite. Quartz occurred in smaller amounts, along with other characteristic peaks of sulfosalt phases (tetrahedrite, pyrite, and bornite) detected in some samples.

4.4. Results obtained by XRF

The results of this analysis showed a notable variability in the chemical composition of the analyzed samples (Table 1). Fe_2O_3 contents were markedly high, reflecting an ore dominated by hematite. MnO reached 0.95% in Sample 06. Relatively low SiO_2 (up to 10.52%) and Al_2O_3 (<1%) contents confirmed a weak quartz gangue. CaO showed variable values, ranging between 0.19% and 41.27%, with significant losses on ignition (LOI) that can reach 32.32%. Finally, the detected SO_3 contents remained also variable values, ranging from 0.03% to 26.09%.

4.5. ICP-OES results

ICP-OES analysis was performed on four samples, selected according to their mineralogical compositions as well as their morpho-structural and textural criteria. It showed high to very high concentrations (ppm) for trace metallic elements, notably Cu (22–6051 ppm), Zn (525–1736 ppm), Sr (134–1152 ppm), Cr (505–1084 ppm), Pb (28–191 ppm), As (13–582 ppm), and Ba (83–53291 ppm). Sulfur (S) is also represented by high concentrations (572-9576 ppm), reflecting a sulfo-salt chemistry. The elements Ti, Zr, Ni and V are expressed in very low concentrations: 47, 14, 12 and 11 ppm, respectively.

4.6. Stable Carbon ($\delta^{13}C$) and Oxygen ($\delta^{18}O$) Isotopes

Isotopic analyses of gangue carbonates (calcite and ankerite) and Jurassic host limestones revealed a relatively wide range of values. Gangue calcite exhibited $\delta^{13}C$ V-PDB (Vienna Pee Dee Belemnite) values ranging from −2.01‰ to −1.46‰, with $\delta^{18}O$ V-SMOW (Vienna Standard Mean Ocean Water) values between +18.21‰ and +20.04‰. Primary calcite (host rock) showed $\delta^{13}C$ V-PDB values ranging from +2.79‰ to +3.53‰, with $\delta^{18}O$ V-SMOW values between +27.14‰ and +28.65‰.

5. DISCUSSION

The micritic, hard, dark gray-blue host rocks of the Jurassic age exhibited a typical conchoidal fracture. They reflected a well-developed early diagenesis. (Flügel, 2004, 2010; Tucker & Wright, 2009). The presence of flint nodules indicates a late silicification process of the carbonate mud (Tucker, 1991; Maliva et al., 2005). Conversely, the occurrence of idiomorphic

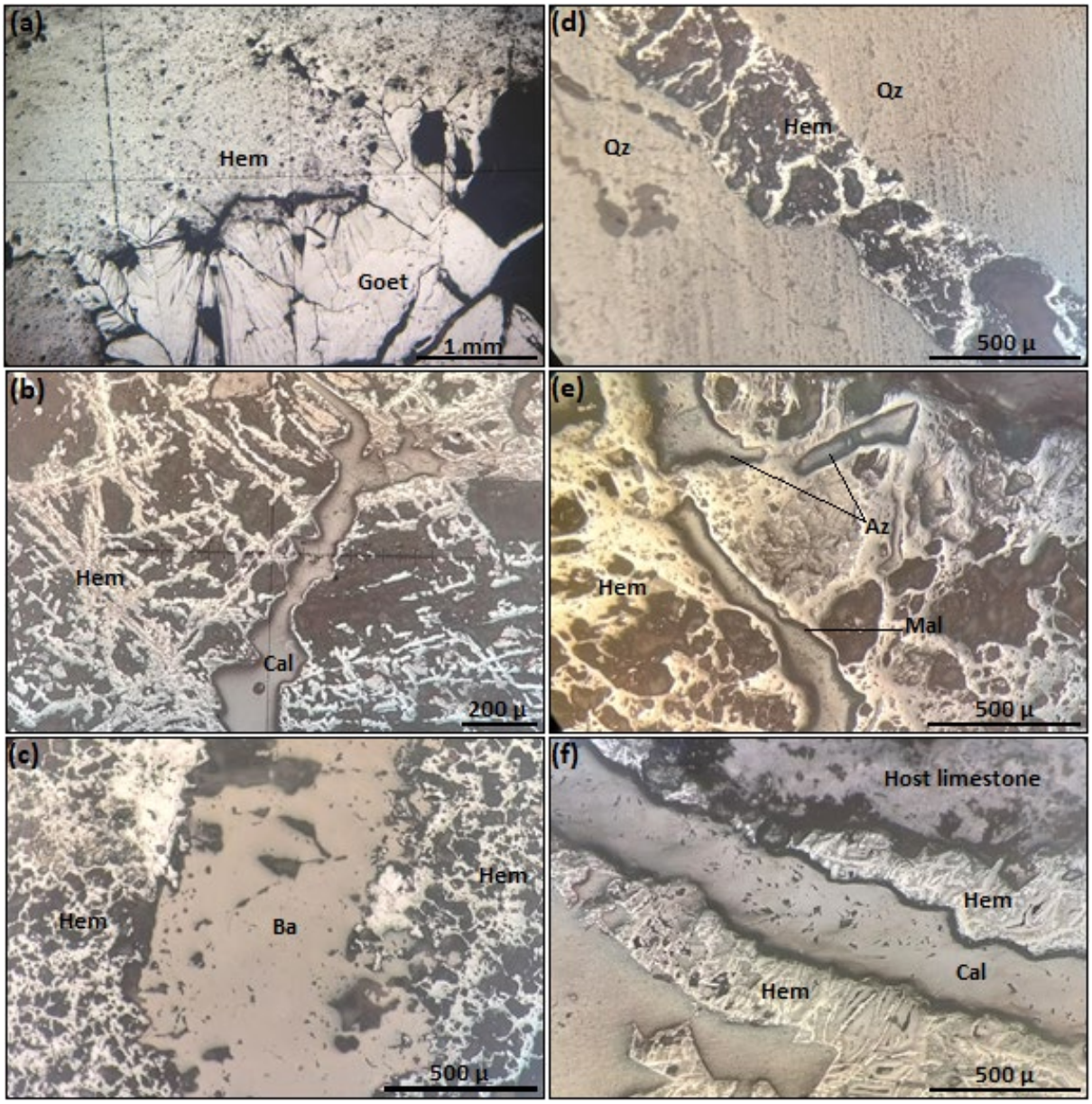

Figure 5. Microphotographs showing the various mineral associations in the Kef Boulehmame iron deposit and their textural features: (a) Hematite (Hem) – goethite (Goet) association; (b) Late calcite vein cutting across the massive lamellar hematite; (c) Barite (Ba) lath cutting across massive hematite; (d) Massive quartz (Qz) cut by a hematite vein; (e) Azurite (Az) – malachite (Mal) association corroded by hematite (Hem); (f) Late hematite and calcite (Cal) filling in a microfracture of the limestone host rock.

Table 1. Results of X-ray fluorescence analysis of samples from the Kef Boulehmame iron ore deposit (in wt. %). CRAPC-Biskra, ORGM-Boumerdes, November 2025.

Sample Number	Contents (%)											
	SiO_2	Al_2O_3	Fe_2O_3	MnO	CaO	MgO	TiO_2	K_2O	Na_2O	P_2O_5	SO_3	LOI
1	10.52	0.49	14.49	0.34	41.27	0.57	<0.05	<0.05	<0.05	<0.05	--	32.32
2	5.28	0.73	72.18	--	3.47	0.51	--	0.51	0.06	--	0.04	17.13
3	2.30	0.20	68.37	--	10.75	0.25	--	0.03	0.01	--	0.03	17.91
4	0.14	0.13	0.29	--	66.72	0.00	--	0.00	0.00	--	26.09	6.60
5	6.17	0.54	70.02	--	9.75	0.20	--	0.75	0.10	--	1.97	11.19
6	2.88	0.58	79.03	0.95	0.19	<0.05	<0.05	<0.05	<0.05	<0.05	--	11.39
7	1.18	0.20	84.73	--	1.46	0.21	--	0.03	0.01	--	0.04	12.04
8	10.06	0.50	75.28	0.57	0.20	<0.05	<0.05	<0.05	<0.05	<0.05	--	11.36
9	1.66	0.57	39.78	0.68	31.20	<0.05	<0.05	<0.05	<0.05	<0.05	--	24.50
10	2.37	0.42	33.44	--	35.20	0.79	--	0.07	0.02	--	4.54	23.05

pyrite crystals within the micrite, suggested reducing conditions that developed during or following this early diagenesis (Raiswell & Canfield, 1998). The mudstone texture with rare poorly fossiliferous wackestones (ostracods, gastropods, and foraminifera) indicated a relatively calm, internal-platform marine depositional environment at moderate to significant water depth (Burchette & Wright, 1992; Tucker & Wright, 2009; Flügel, 2010; Juutinen et al., 2023). From a geochemical perspective, X-ray diffraction analysis revealed bornite (samples 04, 08, and 09), suggesting a minor contribution of copper-bearing sulfide phases within the mineral assemblage (Figure 6).

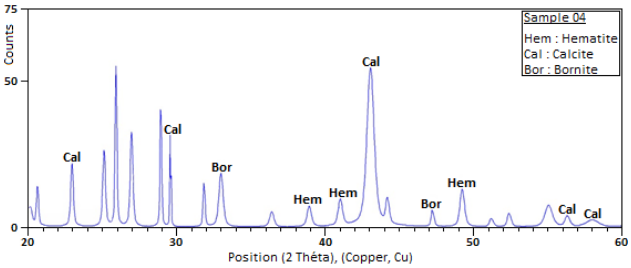

Figure 6. Result of the X-ray diffraction analysis, showing the main mineral phases of sample 4, collected at Kef Boulehmame. CRAPC, Biskra, November 2025.

This specificity may indicate localized hydrothermal activity or secondary mineralization. X-ray fluorescence analysis showed a high Fe_2O_3 content, highlighting the significance of hematite mineralization (Table 1). The proportion of MnO suggested a minor contribution from manganese-bearing minerals (pyrolusite and rhodochrosite). Low SiO_2 content indicated a minor quartz gangue (Figure 7).

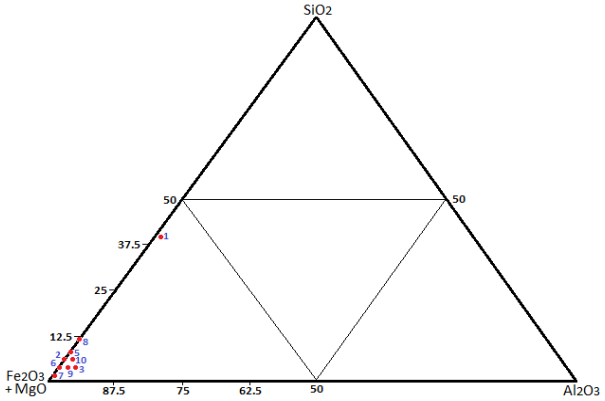

Figure 7. The distribution of samples collected from the iron ore deposit of Kef Boulehmame in the SiO_2-(Fe_2O_3+MgO)-Al_2O_3 diagram.

The relationship between CaO and losses on ignition (LOI) due to the decomposition of carbonate during the melting process owing CO_2 release reflected a predominantly calcitic gangue, in addition to the influence of the carbonate host rocks, particularly near contact zones. SO_3 may be related to bornite, pyrite, or barite, suggesting partial alteration of sulfide phases under supergene oxidizing conditions. The analytical technique of inductively coupled plasma optical emission spectroscopy (ICP-OES) showed relatively high concentrations of Cu, Zn, Pb, As, and Ba, along with a significant sulfur content, indicating a polymetallic hydrothermal contribution (Table 2).

Table 2. Results of the ICP-OES analysis of the Kef Boulehmame iron ore deposit (in ppm). CRAPC-Biskra, ORGM-Boumerdes, October 2025. (< d.l: below the detection limit).

Elements	Sample Number 01	06	08	09
	Contents (ppm)			
Cu	156	22	6051	3768
Pb	34	28	154	191
Zn	525	839	1378	1736
As	13	< d.l.	371	582
Rb	< d.l.	< d.l.	< d.l.	< d.l.
Sr	467	134	244	1152
Ba	32667	83	11692	53291
Mo	< d.l.	< d.l.	< d.l.	< d.l.
Cr	731	505	1074	1084
V	9	4	11	8
Ni	5	5	9	12
Zr	7	2	14	13
Ti	< d.l.	< d.l.	47	46
In	< d.l.	< d.l.	< d.l.	< d.l.
S	7119	572	630	9576

This association, frequently reported in hydrothermal systems, suggested the existence of a late-stage fluid phase responsible for the emplacement of sulfate (barite) mineralizations within the ferriferous ore (Velasco et al., 2013; Vergani, 2022; Damian et al., 2023; Zhao et al., 2024).

Supergene alteration of pre-existing sulfides under acidic conditions may explain the mobilization of these metals through leaching followed by secondary concentration in oxidation minerals or interstitial solutions. The high Sr and Cr contents reflect a mixed inheritance, possibly derived from the carbonate host lithology and external contributions associated to mafic intrusions or the alteration of primary basement rocks near Kef Boulehmame (Santos et al., 2023) (Figure 8).

The analysis of stable C-O isotopes showed slightly negative $\delta^{13}C$ V-PDB values for the gangue calcite (−2.01‰ and −1.46‰), which differed from the typical composition of Jurassic marine carbonates (+1‰ to +3‰ V-PDB). These values exclude direct precipitation from seawater (Friedman & O'Neil, 1977; Veizer et al., 1999; Hollis et al., 2024), and instead favor an inorganic origin from crustal carbon, probably derived from thermal decarbonation of the host carbonates (Taylor, 1974; Veizer & Hoefs, 1976; Ohmoto, 1986; Zheng, 1999; Zhuang et al., 2025).

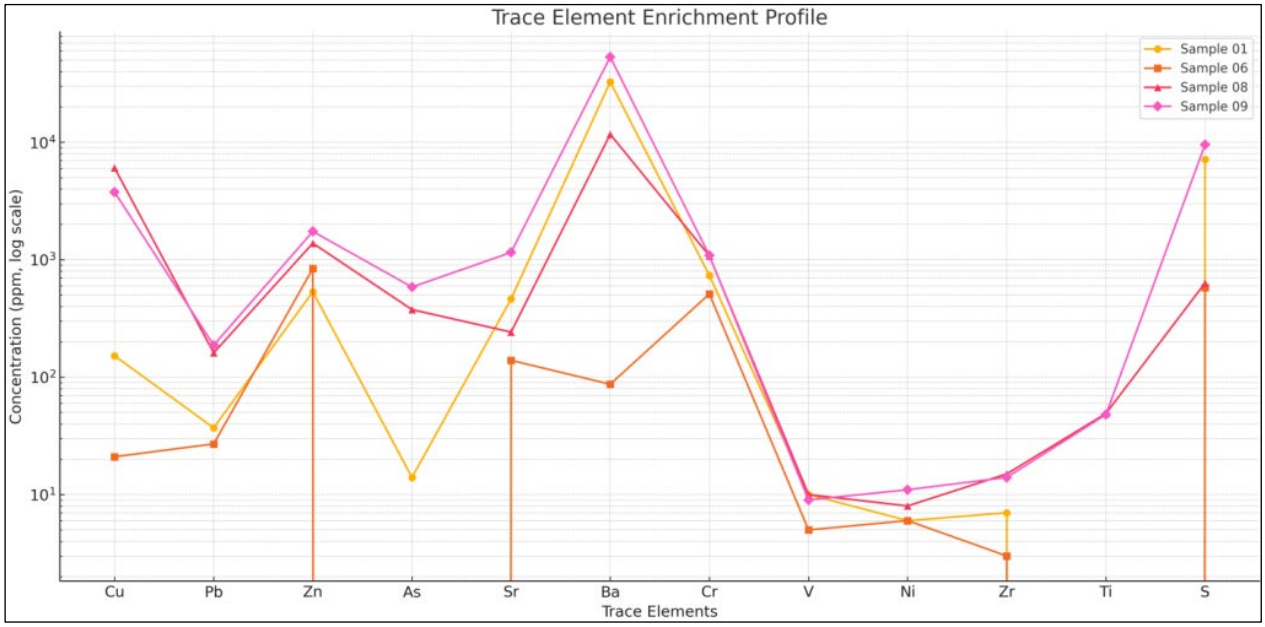

Figure 8. Trace element enrichment profile of the iron-bearing mineralization at Kef Boulehmame based on ICP-OES analysis results. CRAPC-Biskra, ORGM-Boumerdes, October 2025.

Table 3. Isotopic composition of $\delta^{13}C$ and $\delta^{18}O$ of gangue calcite and carbonate host rock. Isotope Geochemistry Laboratory, University of Cologne, Germany. September 2025. Reproducibility of results: ± 0.1‰. To convert $\delta^{18}O$ (PDB) to $\delta^{18}O$ (SMOW), we use the following conversion rule: $\delta^{18}O$ (SMOW) = 1.03092 × $\delta^{18}O$ (PDB) + 30.92.

Sample Number	Mineral	$\delta^{13}C_{(PDB)}$ ‰	$\delta^{18}O_{(PDB)}$ ‰	$\delta^{18}O_{(SMOW)}$ ‰	Brief description
1	Gangue calcite	— 1.46	— 10.54	+ 20.04	Whitish crystalline gangue calcite
2	Gangue calcite	— 1.83	— 11.71	+ 18.84	Ferruginized crystalline gangue calcite
3	Primary calcite	+ 2.79	— 2.19	+ 28.65	Altered limestone, friable, intensely fractured
3 (a)	Primary calcite	+ 2.86	— 2.87	+ 27.95	Altered limestone, with calcitic filling
4	Gangue calcite	— 2.01	— 12.32	+ 18.21	Ferruginized crystalline gangue calcite
5	Primary calcite	+ 3.53	— 3.47	+ 27.34	Lias limestone, micritic, sound, with conchoidal fractures
6	Primary calcite	+ 3.45	— 3.65	+ 27.14	
6 (a)	Primary calcite	+ 3.26	— 3.57	+ 27.23	

This isotopic signature is commonly observed in gangue calcites from hydrothermal fluids that interacted with carbonate rocks, without significant input of oxidized organic matter, which usually gives more negative $\delta^{13}C$ V-PDB values between −5‰ and −10‰ (O'Neil et al., 1969; Oehlert & Swart, 2014; Bougeault et al., 2020; Bodden et al., 2023). Conversely, primary calcite (host rock) showed $\delta^{13}C$ V-PDB values within the range of Jurassic marine carbonates (+2.79‰ to +3.53‰). The same analysis indicated $\delta^{18}O$ V-SMOW values for gangue calcite between +18.21‰ and +20.04‰, significantly lower than the oxygen isotopic composition of Jurassic host limestones (+21‰ to +27‰). These values reflected the impact of interaction between the host rocks and mineralizing fluids, resulting in several epigenetic phases, including iron deposition, dolomitization, and silicification.

The decrease in $\delta^{18}O$ V-SMOW values could be explained by the propagation of a thermal gradient from the ore body toward the surrounding host rocks, that is, the effect of the mineralizing fluid on these carbonates (Holser & Kaplan, 1966; Jensen, 1967; Ohmoto, 1972; Ohmoto & Rye, 1979; Claypool et al., 1980; Ohmoto & Lasaga, 1982; Charef, 1986; Ohmoto & Goldhaber, 1997; Taylor, 1997). This hot, saline, metal-rich fluid, derived from connate waters trapped in deep sediments, has been proposed as the origin of mineralizing fluids in the Boujabeur, Fedj El–Adoum, and Jebel Doghra deposits in Tunisia (Charef & Sheppard, 1991; Sheppard et al., 1996; Jemmali et al., 2011; Zedam, 2012; Bouhlel et al., 2016; Laouar et al., 2016; Zedam et al., 2022). Finally, it is notable that the $\delta^{18}O$ V-SMOW composition of primary calcite (host rocks), ranging from +27.14‰ to +28.65‰, is consistent with that of Jurassic limestones (Table 3).

6. GENESIS OF MINERALIZATION

Ferriferous mineralizations can be generated through multiple processes. Their formation conditions vary according to geological and petro-geochemical contexts (Zhao et al., 2014). Based on the structural and geochemical characteristics of the Kef Boulehmame deposit, hypotheses involving magmatic segregation, skarn-type metasomatism, or chemical sedimentation of iron in banded iron formations (BIF) can be excluded. The $\delta^{13}C$ V-PDB and $\delta^{18}O$ V-SMOW values of the associated gangue calcite support a low-temperature hydrothermal origin, comparable to those recorded in several peri diapiric polymetallic deposits. Examples include Boujabeur, Fedj El–Adoum, and Jebel Doghra in Tunisia and Ouenza, Boukhadra, Mesloula, and Aïn Mimoun in Algeria (Charef & Sheppard, 1991; Sheppard et al., 1996; Bouzenoune & Lécolle, 1997; Jemmali et al., 2011; Aït Abdelouahab et al., 2011; Zedam, 2012; Bouhlel et al., 2016; Laouar et al., 2016; Bakelli et al., 2022; Zedam et al., 2022; Metrouni et al., 2026).

The Kef Boulehmame deposit may also represent an ancient polymetallic system with a high iron content (pyrite, pyrrhotite, chalcopyrite, bornite, and arsenopyrite) but low Pb, Zn, Cu, and Ba concentrations (Vergani, 2022). This interpretation is supported by moderate anomalies in trace metals (Cu, Pb, Zn, Ba, As, and Sr) and sulfur. Intense supergene alteration imparts complexity in terms of paragenetic succession and gives the deposit a distinctive character. The deposit differs from Alvo 118 (Carajás, Brazil), Las Cruces (Iberian Pyrite Belt, Spain), Jbel Rhals (Eastern High Atlas, Morocco), and Lombard (Italy), where iron concentrations in gossans are derived directly from the oxidation of preserved primary sulfides (Velasco et al., 2013; Yesares et al., 2017; Verhaert et al., 2018; Vergani, 2022; Santos et al., 2023).

Regionally, the deposit shows analogies with Kherzet Youcef, Ouenza, Boukhadra, Zaccar, and Chaabet El Bellout, where oxidized ferriferous mineralization results from the supergene alteration of siderite (Hanssen & Bourezg, 1990; Aït Abdelouahab et al., 2011; Chaa & Boutaleb, 2016; Zerrouki et al., 2022). The low SiO_2 and Al_2O_3 contents distinguish this deposit from lateritic ferruginous crusts rich in SiO_2 and Al_2O_3, which occur in humid tropical regions (Reichert & Borg, 2008; Jemmali & Souissi, 2018; El Ghastalany et al., 2023).

Supergene oxidation of sulfide mineralization causes sulfide dissolution under acidic, oxidizing conditions, enriching the environment with metallic cations that behave differently according to their mobility (Taylor, 2011; Gao et al., 2020; Niesiobędzka, 2023; Kaba et al., 2023). This process controls the mineralogical composition and chemistry of the gossans and explains the zoning observed in supergene alteration profiles of polymetallic deposits. The scarcity of secondary minerals in the deposit can be attributed to two factors: (a) total leaching of metals as cations under acidic, oxidizing conditions (surficial-leached capping zone), and (b) the lack of petrogeochemical data, primarily due to the absence of deep exploration. These conditions hinder the proposal of a precise genetic model for the formation of ferriferous mineralization at Kef Boulehmame.

7. CONCLUSION

The petro-mineralogical and geochemical study of the Kef Boulehmame deposit demonstrates that the mineralization exhibits a relatively simple paragenesis, dominated by iron oxy-hydroxides (hematite, goethite, and limonite), accompanied by rare sulfides (pyrite and bornite) and occasionally sulfosalts (tetrahedrite). The gangue primarily comprises calcite, associated with barite and quartz.

The entire mineralization occurs within a Jurassic micritic limestone host with mudstone to wackestone textures characteristic of a carbonate platform, indicating a relatively deep marine environment and providing a favorable lithological metallotect for the emplacement of this type of mineralization.

From a geochemical perspective, the ore exhibits high Fe_2O_3 and CaO contents, moderate SiO_2 and SO_3 concentrations, and low to very low levels of Al_2O_3, MnO, MgO, TiO_2, K_2O, Na_2O, and P_2O_5. Trace metal concentrations (Cu, Zn, Pb, Sr, Cr, Ti, Zr, Ni, and V) together with sulfur and barium indicate a polymetallic hydrothermal contribution. Isotopic values of $\delta^{13}C$ V-PDB and $\delta^{18}O$ V-SMOW measured in the gangue calcite suggest precipitation from low- to moderate-temperature hydrothermal fluids interacting with the host carbonates, without significant input from organic matter. The proposed genetic model involves four main factors allowing the iron deposit formation:

(1) the lithological nature of the porous and reactive carbonate host rock,

(2) the fracturing system that facilitates the circulation of hydrothermal fluids,

(3) the ascent of likely multiphase iron-rich hydrothermal fluids, followed by:

(4) a partial or limited contribution from the supergene alteration phase, which led to the formation of iron oxides and hydroxides.

These results provide new constraints on fluid origins and depositional conditions, offering a foundation for refining exploration strategies in similar geological environments. Furthermore, the increase in the number of samples analyzed, combined with the

expansion of the study area and the deployment of advanced analytical techniques (microthermometry, laser ablation ICP-MS), contributes to the improvement of interpretation accuracy.

Adopting such an approach will certainly yield reliable scientific results that are widely recognized for their high reproducibility. Finally, the data obtained in this study, along with their interpretations, represent a preliminary framework for future investigations of analogous deposits associated with hydrothermal systems.

Acknowledgements

We would like to express our gratitude and heartfelt thanks to all the colleagues who helped us draft this preliminary petrogeochemical study regarding the iron mineralization of Kef Boulehmame. First of all, we must thank Professor Frédéric BOULVAIN, Liège -Sart Tilman Campus, for his efforts in conducting the isotopic analyzes at the University of Cologne, Germany. We must not forget, of course, the heads of the geochemistry and geology laboratories at the ORGM in Boumerdès, as well as those at the CRAPC in Biskra.

REFERENCES

Aïssa, D.E., Marignac, C., Cheilletz, A. & Gasquet, D., 1998. *Géologie et métallogénie sommaire du Massif de l'Edough (NE Algérie).* Mém. Serv. Géol. Alg. N.09. P. 7-55.

Aït Abdelouahab, D., Bouzenoune, A., & Preat, A., 2011. *Les isotopes stables du carbone et de l'oxygène des carbonates (calcaires et siderites) du gisement de fer de Boukhadra (Algérie nord oriental).* Bulletin du Service Géologique l'Algérie Volume 22, Numéro 3, Pages 381-395. https://asjp.cerist.dz/en/article/1126.

Bakelli, A., Sami, L., Boutaleb, A., Kolli, O., Haddouche, O., Demir, Y., & Zedef, V., 2022. *Evolution and genesis of fluorite mineralization in the Ouenza region (North-East of Algeria): evidence from fluid inclusions and stable isotopes (C, O, and S).* Arab J Geosci., 15: 514. https://doi.org/10.1007/s12517-022-09726-8.

Bekker, A., Slack, J.F., Planavsky, N., Krapez, B., Hofmann, A., Konhauser, K.O., & Rouxel, O.J., 2010. *Iron Formatio: The sedimentary product of a complex interplay among mantle, tectonic, oceanic and biospheric processes.* Economic Geology, 105, 467-508. https://doi.org/10.2113/gsecongeo.105.3.467.

Bodden, T.J., Bornhorst, T.J., Bégué, F., & Deering, C., 2023. *Sources of Hydrothermal Fluids Inferred from Oxygen and Carbon Isotope Composition of Calcite, Keweenaw Peninsula Native Copper District, Michigan, USA.* Minerals, 12, 474. https://doi.org/10.3390/min12040474.

Bouchair, B., Bouzenoune, A., Benmebarek, O., & Belhimer, Z., 2021. *The iron ore resources of northern Algeria. Typology, geological contexts, and geochemical characteristics.* La 1ère édition des Journées Internationales en Géosciences et Environnement (JIGE 2021), 26 et 27 mars 2021, Agadir, Maroc.

Bouftouha, Y., 2000. *Caractères pétrographiques, minéralogiques et géochimiques du skarn de la d'Aïn-Sedma (Cap Bougaroun, nord-est algérien).* Bulletin du Service Géologique de l'Algérie. Vol.11, n° 2, pp.119 - 144, 11 Fig., 4 Tab., 2 pl.

Bougeault, C., Durlet, C., Vennin, E., Muller, E., Ader, M., Ghaleb, B., Gérard, E., Virgone, A., & Gaucher, E.C., 2020. *Variability of Carbonate Isotope Signatures in a Hydrothermally Influenced System: Insights from the Pastos Grandes Caldera (Bolivia).* Minerals, 10, 989; https://doi:10.3390/min10110989.

Bouhlel, S., Leach, D.L., Craig, A.J., Marsh, E., Salmi-Laouar, S., & Banks, D.A., 2016. *A salt diaper-related Mississippi Valley-type deposit: the Bou Jaber Pb-Zn-Ba-F deposit, Tunisia: fluid Inclusion and isotope study.* Miner Deposita. https://doi.org/10.1007/s00126-015-0634-8.

Bouillin, J. P., 1977. *Géologie alpine de la petite kabylie dans les régions de Collo et d'El Milia.* Thèse de doctorat d'état, université de Paris VI (Pierre et Marie Curie), 511p.

Bouzenoune, A., & Lécolle, P., 1997. *Petrographic and geochemical arguments for hydrothermal formation of the Ouenza siderite deposit (NE Algeria).* Miner Deposita 32:189–196.

Burchette, T.P., & Wright V.P., 1992. *Carbonate ramp depositional systems.* Sediment. Geol., 79: 3-57. https://doi.org/10.1016/0037-0738(92)90003-A.

Chaa, H., & Boutaleb, A., 2016. *Mineralogical and geochemical characteristics of the Zaccar Fe-(Ba-Pb-Zn-Cu) deposit in Ain Defla, Algeria. (Northwestern Algeria).* Arab J. Geosci., 9:266.

Chaib, A., Bouabdallah, S., Ferfar, M., Benselhoub, A., Dovbash, N., & Bellucci, S., 2024. *Investigation of physicochemical characterization and magnetic enrichment of iron ore from Sidi Maarouf deposit.* Technology Audit and Production Reserves, 1 (3(75)), 9–14. https://doi.org/10.15587/2706-5448.2024.297846.

Charef, A., 1986. *La nature et le rôle des phases fluides associées à la minéralisation Pb-Zn dans les formations carbonatées et leurs conséquences métallogéniques : étude des inclusions fluides et des isotopes (H, C, O, S, Pb) des gisements des Malines (France), Jbel Hallouf-Sidi Bou Aouane et Fedj-el-Adoum (Tunisie).*Thèse d'Etat, INPL – CRPG, Nancy, France, 303 p.

Charef, A., & Sheppard, S. M. F., 1991. *The diapir related Bou Grine Pb-Zn deposit (Tunisia): evidence for the role of hot sedimentary basin brines.* In M. Pagel et J. Loroy (eds): Source, Transport and deposition of metals. Belkema, Rotterdam, pp. 269-272.

Claypool, G. E., Holser, W.T., Kaplan, I. R., Sachet, H., & Zak, I., 1980. *The age curves of sulfur and Oxygen isotopes in marine sulphate and their Mutual interpretation.* Chemical Geology, 28, pp. 199-260.

Cooper, A.H., Brown, T.J., Price, S.J., Ford, J.R., & Waters, C.N., 2018. *Humans are the most significant global geomorphological driving force of the 21st century.* The Anthropocene Review p8.

Damian, G., Apopei, A. I., Buzatu, A., Maftei, A. E., & Damian, F., 2023. *New Mineral Occurrences in Massive Sulfide Deposits from Măniilă, Eastern Carpathians, Romania*, 13 (1), 111. https://doi.org/10.3390/min13010111.

Diab, H., Chouabbi, A., Chi Fru, E., Nacer, J.-E., & Krekeler, M., 2020. *Mechanism of formation, Mineralogy and geochemistry of the ooidal ironstone of Djebel Had, Northeastern Algeria.* Journal of African Earth Sciences.

https://doi.org/10.1016/j.jafrearsci.2019.103736.

Dunham, R.J., 1962. *Classification of carbonate rocks according to depositional textures. In: Classification of Carbonate Rocks (Ed. W.E. Ham).* Am. Assoc. Pet. Geol. Mem., 1, 108–121.

Durand-Delga, M., 1955. *Etude géologique de l'Ouest de la chaîne numidique (Thèse Paris).* Bull. Serv. Carte géol. Algérie, 2ème Série, stratigraphie, descriptions régionales, № 24, 533 p. Alger.

Durand-Delga, M., 1969. *Mise au point sur la structure du Nord-Est de la Berbérie.* Publ. Serv. Géol. Algérie, n.39, 89-131.

Durand-Delga, M., Rossi, P., Olivier, P., & Puglisi, D., 2000. *Structural setting and ophiolitic nature of Jurassic basic rocks associated with the Maghrebian flyschs in the Rif (Morocco) and Sicily (Italy). C. R. Acad. Sci., Série IIA.*

El Ghastalany, R., Branquet, Y., Bagga, M.A., Taviche, I. K., Wafik, A., Ghnahalla, M., & Abdeina, E.H., 2023. *Nature et origine des cuirasses ferrugineuses de la région de Khat Oummat Elbid, Inchiri, Mauritanie.* BSGF – Earth Sciences Bulletin 2023, 194,3. https://doi.org/10.1051/bsgf/2023002.

Flügel, E., 2004. *Microfaciès of carbonates rocks. Analysis, Interpretation and Application.* Springer (1st edition).

Flügel, E., 2010. *Microfaciès of carbonates rocks. Analysis, Interpretation and Application.* Springer (2nd edition).

Folk, R. L., 1959. *Practical petrographic classification of limestones.* AAPG Bulletin, 43 (1) ,1-38.

Friedman, I., & O'Neil, J.R., 1977. *Compilation of Stable Isotope Fractionation Factors of Geochemical Interest.* U.S. Geol. Surv. Professional Paper 440- KK, Data of Geochemistry, 6th Edition.

Gao, L., Li, R., Liang Z., Wu, Q., Yang, Z., Li, M., Chen, J., & Hou, L., 2020. *Mobilization mechanisms and toxicity risk of sediment trace metals (Cu, Zn, Ni, and Pb) based on diffusive gradients in thin films: A case study in the Xizhi River basin, South China.*Journal of Hazardous Materials. https://doi.org/10.1016/j.jhazmat.2020.124590.

Hanssen, E. & Bourezg, M., 1990. *Geology and geochemistry of gossans and ironstones in carbonate and alumino-silicate environments in northeastern Algeria.* Journal of Geochemical Exploration, 38, 323-349.

Heimann, A., Beard, B.L., & Johnson, C.M., 2020. *Fe isotope fingerprints of ore-forming processes. Annual Review of Earth and Planetary Sciences,* 48, 491–519.

Hollis, S.P., Dennis, P.F., Menuge, J.F., Doran, A.L., Marca, A., Davidheiser-Kroll, B., Wilkinson, J.J., Snell, K.E., Turner, O., Güven, J., & Boyce, A., 2024. *Tracking fluid temperature and $\delta^{18}O$ in carbonate-hosted hydrothermal ore systems using clumped C-O isotopes.* Economic Geology, 119(6), 1369–1382.

Holser, W. T., & Kaplan, I. R., 1966. *Isotope geochemistry of sedimentary sulfates.* Chem. Geol., 1 pp. 93-135.

Idoine, N.E., Raycraft, E.R., Shaw, R.A., Hobbs, S.F., Deady, E.A., Everett, P., Evans, E.J., & Mills A.J., 2022. *World Mineral Production 2016–20.* British Geological Survey.

Jemmali, N., & Souissi, F., Villa, I.M., Vennemann, T., 2011. *Ore genesis of Pb–Zn deposits in the Nappe zone of Northern Tunisia: Constraints from Pb-S-C-O isotopic systems.* Ore Geology Reviews*, p11.* https:// doi.org/10.1016/j.oregeorev.2011.04.005.

Jemmali, N., & Souissi, F., 2018. *Lead Isotopes as Tracers of Metal Sources and Timing of the Carbonate-Hosted Pb-Zn Deposits in the Nappes Zone, Northern Tunisia.* Contributions to Mineralization. In Tech. https:/ / doi.org/10.5772/in tech open.72690.

Jensen, M. L., 1967. *Sulfur isotopes and mineral genesis.* In: H. L. Barnes (Editeur), Geochemistry of Hydrothermal Ore Deposits. Holt, Rinehart and Winston, New York, pp.143 – 165.

Juutinen, M., Seitsaari, M., & Sarala, P., 2023. *Geochemical and mineralogical characterization of mine tailings at the Rautuvaara mine site and aspects to environmental conditions and resource potential.* Bulletin of the Geological Society of Finland, Vol. 95, 2023, pp 59–78. https://doi.org/10.17741/bgsf/95.1.005.

Kaba, O.B., Souissi, F., Keita, D., Filippov, L.O., Conté, M.S.M., & Kanari, N., 2023. *Mineral Weathering and Metal Leaching under Meteoric Conditions in F-(Ba-Pb-Zn) Mining Waste of Hammam Zriba (NE Tunisia).* Materials, 16 (23), 7443. https://doi.org/10.3390/ma16237443.

Laouar, R., Salmi-Laouar, S., Sami, L., Boyce, A.J., 2016. *Fluid inclusion and stable isotope studies of The Mesloula Pb-Zn-Ba ore deposit, NE Algeria: Characteristics and origin of the mineralizing fluids.* Journal of African Earth Sciences. DOI:10.1016/j.jafrearsci.2016.06.004

Liu, S., & Lin, M., 2024. *Trade dynamics of ferrous metals in emerging and developing countries*. Resources Policy, Volume 90, 104742. https://doi.org/10.1016/j.resourpol.2024.104742.

Maliva, R.G., Knoll, A.H., & Simonson, B.M., 2005. *Secular change in the Precambrian silica cycle: Insights from chert petrology.* Geological Society of America v. 117; no. 7/8; p. 835–845. https://doi: 10.1130/B25555.1

Mallinger, K., & Mergili, M., 2020. *The global iron industry and the Anthropocene.* The Anthropocene Review 1–19.

Metrouni, H., Laouar, R., Zedam, R., Bouhlel, S., & Tlili, A., *2026. Hydrothermal alteration features of the peridiapiric Pb-Zn-Ba deposits of Northeastern Algeria: Geochimical approach and stable C and O isotope study. Carbonates and Evaporates (2026) 41:37.* https://doi.org/10.1007/s13146-026-01247-9.

Mowafa, T., 2014. *The Mineral Industry of Algeria.* U.S. Geological Survey Minerals Yearbook.

Mowafa, T., 2018. *The Mineral Industry of Algeria.* U.S. Geological Survey Minerals Yearbook.

Niesiobędzka, K., 2023. *Mobility indexes of Cu, Pb, and Zn in soil ecosystems with various levels of metal contamination (in Poland).* Environ Monit Assess, 195:505. https://doi.org/10.1007/s10661-023-11069-0.

Oehlert, A.M., & Swart, P.K., 2014. *Interpreting carbonate and organic carbon isotope covariance in the sedimentary record.* Nature Communications. 5 :4672. https://doi.org/10.1038/ncomms 5672.

Ohmoto, H., 1972. *Systematics of sulfur and carbon isotopes in hydrothermal ore deposits.* Econ. Geol., 67, pp. 551-579.

Ohmoto, H., & Rye, R.O., 1979. *Isotopes of sulphur and carbon.* In: H.L. Barnes (Editor), Geochemistry of hydrothermal Ore Deposits. Wiley, New York, N.Y., 2nd ed., pp. 509-567.

Ohmoto, H., & Lasaga, A. C., 1982. *Kinetics of reactions between aqueous sulfates and sulfides in hydrothermal systems.* Geochi. Cosmochim. Acta, 46, pp. 1727-1745.

Ohmoto, H., 1986. *Stable isotope geochemistry of ore deposits.* Reviews in Mineralogy 16, 491–559.

Ohmoto, H., & Goldhaber, M. B., 1997. *Sulfur and carbon*

isotopes. In: Barnes, H. J. (editor) Geochemistry of hydrothermal ore deposits. Third edition, Wiley-Interscience, New York, pp.313-327.

O'Neil, J.R., Clayton, R.N., & Mayeda, T.K., 1969. *Oxygen isotope fractionation in divalent metal carbonates*. J. Chem. Phys. 51, 5547. https://doi: 10.1063/1.1671982.

Raiswell, R., & Canfield, D.E., 1998. *Sources of iron for pyrite formation in marine sediments.* American Journal of Science, 298 (3), 219-245. https://doi.org/10.2475/ajs.298.3.219.

Reichert, J., & Borg, G., 2008. *Numerical simulation and a geochemical model of supergene carbonate-hosted non sulphide zinc deposits.* ogr 33, 20 pages.

Santos, P.H.C.d., Costa, M.L.d., & Roerdink, D.L., 2023. *Geochemical and Isotopic Fractionation in The Hypogene Ore, Gossan, and Saprolite of the Alvo 118 Deposit: Implications for Copper Exploration in the Regolith of the Carajás Mineral Province.* Minerals, 13, 1441. https://doi.org/10.3390/min13111441.

Sheppard, S.M.F., Charef, A., & Bouhlel, S., 1996. *Diapirs and Zn-Pb mineralisation: A general model based on Tunisian (N. Africa) and Gulf Coast (U.S.A.) deposits.* Soc. Of Geol. Special Publication, n°4, pp. 230-243.

Sonarem, 1974. *Rapport géologique sur l'activité de prospection pour le minerai de fer dans le secteur de Sidi Marouf et Kef Boulehmame.* Rapport Inédit.

Taylor, H.P., 1974. *The Application of Oxygen and Hydrogen Isotope Studies to Problems of Hydrothermal, Alterationan Ore Deposition*. Economic Geology Vol. 69, 1974, pp. 843-883.

Taylor, H. P. Jr., 1997. *Oxygen and hydrogen isotope relationships in hydrothermal mineral deposits.* In: Barnes, H.L. (Ed.), Geochemistry of hydrothermal ore deposits. 3rd edition, New York, John Wiley and Sons, 229-302.

Taylor, R., 2011. *Gossans and Leached Cappings Field Assessment.* (1st edition); Springer: Townsville, Australia.

Tucker, M.E., 1991. *Sedimentary Petrology: An Introduction to the Origin of Sedimentary Rocks.* Black well Science.

Tucker, M.E., & Wright, V.P., 2009. *Carbonate sedimentology (2nd edition).* Wiley-Black well.

Veizer, J., & Hoefs, J., 1976. *The nature of O^{18}/O^{16} and C^{13}/C^{12} secular trends in sedimentary carbonate rocks.* Geochimica et Cosmochimica Acta 1976. Vol. 40, pp. 1387 to 1395.

Veizer, J., Ala, D., Azmy, K., Bruckschen, P., Buhl, D., Bruhn, F., Carden, G.A.F., Diener, A., Ebneth, S., Godderis, Y., Jasper, T., Korte, C., Pawellek, F., Podlaha, O.G., & Strauss, H., 1999. *$^{87}Sr/^{86}Sr$, $\delta^{13}C$ and $\delta^{18}O$ evolution of Phanerozoic seawater.* Chemical Geology 161(1):59–88.

Velasco, F., Herrero, J.M., Suàrez, S., Yusta, I., Alvaro, A., & Tornos, F., 2013. *Supergene features and evolution of gossans capping massive sulphide deposits in the Iberian Pyrite Belt.* Ore Geology Reviews. http://dx.doi.org/10.1016/j.oregeorev.2013.01.00

Vergani, F., 2022. *A preliminary petrographic and LA- ICP-MS trace elements study of the iron sulfide- Rich deposits of Lombard Southern Alps: evidences of a hydrothermal origin?* Periodico di Mineralogia. 91, 201- 224.

Received: 20. 04. 2026
Revised: 14. 07. 2026
Accepted: 25. 07. 2026
Published: 31. 07. 2026

Verhaert, M., Bernard, A., Saddiqi, O., Dekoninck, A., Essalhi, M., & Yans, Y., 2018. *Mineralogy and Genesis of the Polymetallic and Polyphased Low Grade Fe-Mn-Cu Ore of Jbel Rhals Deposit (Eastern High Atlas, Morocco).* Minerals 8, 39. https://doi:10.3390/min 8020039.

Vila J.M., 1980. *La chaîne alpine d'Algérie orientale et des confins Algéro-Tunisiens.* Thèse de doctorat d'état, université Pierre et Marie Curie – Paris VI, 663p.

Wang, C., Johnson, C.M., & Beard, B.L., 2019. *Iron isotope fractionation during hydrothermal alteration of basalts: Implications for Fe cycling in submarine systems. Geochimica et Cosmochimica Acta,* 252, 145–163.

Yesares, L., Saez, R., D'Almodóvar, G.R., Nieto, J.M., Gomez, C., & Ovejero, G., 2017. *Mineralogical evolution of the Las Cruces gossan cap (Iberian Pyrite Belt): from subaerial to underground Conditions.* Ore Geology Reviews 80, 377- 405. https://hero.epa.gov/reference/3468305/

Zedam, R., 2012. *Mise en place d'une Minéralisation Hydrothermale au flanc nord de l'anticlinal de Khenchela. Identification et détermination sur fond lithostratigraphique et Tectonique.* Thèse de Doctorat sciences, Univ. Mentouri, FSTGAT, Département des sciences géologiques, Campus Zouaghi Slimane. Juillet 2012, 220 pages. https://fac.umc.edu.dz/fst/fichiers/Geologie.pdf

Zedam, R., Laouar, R., Lekoui, A., Metrouni, H., Bouhlel, S., Boyce, A.J., & Fallick, A.E., 2022. *Origin of the Mizab barite vein-type deposit, Ain Mimoun (NE Algeria): evidence from fluid inclusion and S-, O- and C-stable isotope studies.* Arabian Journal of Geosciences. https://doi.org/10.1007/s12517-022-09611-4

Zerrouki, T., Boutaleb, A., Sami, L., Semchaoui, A.A. & Chabbi, A., 2022. *Study of metasomatose iron deposit of Chaabet El Bellout (Ain Zana, NE of Algeria): mineralogy, geochemistry, and genetic model.* Arab. J. Geosci 15, 1766. https://doi.org/10.1007/s12517-022-11057-7

Zhao, Y., Feng, C., & Li, D., 2014. *The Major Ore Clusters of Super-Large Iron Deposits in the World, Present Situation of Iron Resources in China, and Prospect.* Acta Geologica Sinica, Vol. 88 No 6pp.1895-1915.

Zhao, L., Santosh, M., & Tang, S., 2021. *Global metallogeny, lithospheric architecture and tectonics. Ore Geology Reviews,* 134, 104184.

Zhao, K., Wu F., Cheng, X., Cheng, S., Wu, J., He, Y., Wang, C., Lkebir, N., Cui, S., Hu, P., Wang, J., Xiang, P., & Liu, J., 2024. *Trace Element Compositions of Galena and Cerussite from the Bou Dahar MVT District, Morocco: Insights from LA-ICP-MS Analyses.* Minerals 14 (8): 748. https:/ /doi. org/10.3390/min1 4080748.

Zheng, Y.F., 1999. *Oxygen isotope fractionation in carbonate and sulfate minerals.* Geochemical Journal, 33, 109–126. https://doi.org/10.2343/geochemj.33.109

Zhuang, L., Song, Y., Liu, Y., Deng, T., & Hou, Z., 2025. *Nonsulfide Zn–Pb mineralization and Vertical zoning in the world-class Angouran deposit, NW Iran: linked to water table- controlled supergene processes.* Miner Deposita. https://doi.org/10.1007/s00126-025-01372-w.